Magnetic borophenes from an evolutionary search

Meng-Hong Zhu,[1,*] Xiao-Ji Weng,[1,*] Guoying Gao,[2] Shuai Dong,[3] Ling-Fang Lin,[3] Wei-Hua Wang,[4] Qiang Zhu,[5] Artem R. Oganov,[6,7,8] Xiao Dong,[1,†] Yongjun Tian,[2] Xiang-Feng Zhou,[1,2,‡] and Hui-Tian Wang[1,9]

[1]*Key Laboratory of Weak-Light Nonlinear Photonics and School of Physics, Nankai University, Tianjin 300071, China*

[2]*Center for High Pressure Science, State Key Laboratory of Metastable Materials Science and Technology, School of Science, Yanshan University, Qinhuangdao 066004, China*

[3]*School of Physics, Southeast University, Nanjing 211189, China*

[4]*Department of Electronic Science and Engineering, Tianjin Key Laboratory of Photo-Electronic Thin Film Device and Technology, Nankai University, Tianjin 300071, China*

[5]*Department of Physics and Astronomy, High Pressure Science and Engineering Center, University of Nevada, Las Vegas, Nevada 89154, USA*

[6]*Skolkovo Institute of Science and Technology, 3 Nobel Street, Moscow 143026, Russia*

[7]*Moscow Institute of Physics and Technology, Dolgoprudny, Moscow Region 141700, Russia*

[8]*International Center for Materials Discovery, Northwestern Polytechnical University, Xi'an 710072, China*

[9]*National Laboratory of Solid State Microstructures and Collaborative Innovation Center of Advanced Microstructures, Nanjing University, Nanjing 210093, China*

(Received 5 September 2018; revised manuscript received 23 April 2019; published 10 May 2019)

A computational methodology based on *ab initio* evolutionary algorithms and spin-polarized density functional theory was developed to predict two-dimensional magnetic materials. Its application to a model system borophene reveals an unexpected rich magnetism and polymorphism. A metastable borophene with nonzero thickness is an antiferromagnetic semiconductor from first-principles calculations, and can be further tuned into a half-metal by finite electron doping. In this borophene, the buckling and coupling among three atomic layers are not only responsible for magnetism, but also result in an out-of-plane negative Poisson's ratio under uniaxial tension, making it the first elemental material possessing auxetic and magnetic properties simultaneously.

DOI: 10.1103/PhysRevB.99.205412

I. INTRODUCTION

Two-dimensional (2D) magnetic materials have attracted huge interest owing to their potential applications in spintronics and data storage [1–12]. The ultimate thinness changes the physical properties dramatically compared to the corresponding bulk materials. Although a number of 2D magnetic materials have been proposed theoretically [9–14], few of them were synthesized experimentally. Recent experimental studies found that 2D forms of CrI_3 and $Cr_2Ge_2Te_6$ can inherit the ferromagnetic (FM) order at low temperatures from their bulk forms [1,2]. Strikingly, even for paramagnetic (PM) bulk material, i.e., VSe_2, its monolayer form shows an unexpected strong room-temperature ferromagnetism on van der Waals substrates [3]. Stimulated by these exiting experimental reports, 56 new magnetically ordered monolayer structures were predicted from high-throughput computation to be exfoliable from known magnetic bulk materials [4]. However, discovering new 2D magnetic materials beyond exfoliation from the parent bulk compounds is still governed by trial and error approaches. Among the light element-based 2D materials, graphene is not magnetic [15], but may be a promising material for spintronics by optimizing defects, substrate, or adsorbing hydrogen atoms [16–19]. Boron, with only three valence electrons, is electron-deficient, resulting in the formation of multicenter B-B bonds and rich polymorphism with great chemical complexity in borophenes [20–31]. Various borophenes have been successfully synthesized on Ag, Cu, or Al substrates under ultrahigh-vacuum conditions [32–36]. The atomically thin borophenes display remarkable properties, such as the emergence of superconductivity, massless Dirac fermions, superior transport, and mechanical properties [20–36]. However, the phase diagram of borophene remains largely unexplored. With the goal of uncovering more 2D intrinsically magnetism with superior properties, in contrast to materials made magnetic by magnetic doping [29–31], we developed a new strategy based on evolutionary structure prediction and explored the magnetic borophenes in a systematic manner.

II. METHOD

To search for the stable 2D magnetic structures, we further developed a new computational scheme based on the *ab initio* evolutionary algorithm USPEX [37–40] combined with spin-polarized density functional theory (DFT). The initial structures are randomly produced with assigned layer group symmetry and user-defined thickness. They are assumed to have either FM, antiferromagnetic (AFM), or nonmagnetic (NM) order. The corresponding values of magnetic moments are then set as 1 for low spin (LS), 4 for high spin state (HS) with the signs (+ or −) depending on FM or AFM, or 0 for NM. The ratios of different structures (NM, FM-LS,

*These coauthors contributed equally to this work.
†xiao.dong@nankai.edu.cn
‡xfzhou@nankai.edu.cn; zxf888@163.com

FM-HS, AFM-LS, AFM-HS, FM-LSHS, and AFM-LSHS) is also a user-defined parameter [41]. Random structures with an odd number of atoms are supposed to have FM order automatically. For the evolutionary search, either the relaxed energy or the total magnetic moment was used as a criterion (*fitness* function) for parent structure selection to generate new structures by various evolutionary operators, such as heredity and mutations (lattice mutation, soft-mode mutation, spin mutation). The optimized individual magnetic moments are saved for further data processing by new operators of spin heredity or spin mutations, which allow us to find optimal magnetic order. For an intrinsic magnetic system, e.g., CrI_3, the total energy was selected as the criterion to find the most thermodynamically stable structure. By contrast, for the nonmagnetic system, e.g., borophene, there are several alternative ways to be considered: (i) If the energy was selected as the criterion, the target is to find the lowest-energy structure associated with a few magnetic phases since boron is an intrinsic NM element. (ii) While the total magnetic moment was chosen, the target is to find a structure with the largest magnetic moment. Hence many metastable magnetic borophenes are obtained. However, the most magnetic phase has high energy and its synthesis is unrealistic. (iii) To find a suitable magnetic lower-energy structure, we can define fitness $= (E_{\text{tot}} - a|\text{spin}|)/n$. Here E_{tot}, $|\text{spin}|$, and n are the total energy, total magnetic moment, and number of atoms for the whole system, and such search worked well with $a = 2$ eV/μ_B. For each relaxed structure, we sum over the (absolute) values of the magnetic moments for all atoms ($\sum M_i$ and $\sum |M_i|$). If $\sum |M_i|$ is close to zero ($<0.03 \times N_{\text{atoms}}$, where N_{atoms} is the number of magnetic atoms), we assign it to be NM; otherwise, the structure would be either AFM ($|\sum M_i| < 0.25 \times N_{\text{atoms}}$) or FM ($|\sum M_i| \geqslant 0.25 \times N_{\text{atoms}}$). We also assign the structure to be LS {if $\max(|M_i|) < 1.5$} or HS {$\min(|M_i|) > 1.5$}. Otherwise, the structure would be labeled as a hybrid HSLS. We limited our structure search by primitive cell of 5–20 atoms; starting thickness of the vacuum region was 20 Å. Structure relaxations and total energy calculations were performed with the projector-augmented wave [42] (PAW) method as implemented in the VASP package, [43] and the exchange-correlation energy was computed within the generalized gradient approximation (GGA) with the functional of Perdew, Burke, and Ernzerhof (PBE) [44]. The plane-wave cutoff energy of 600 eV and uniform Γ-centered k-point grids with the resolution of $2\pi \times 0.025$ Å^{-1} were used. The convergence for terminating the electronic self-consistency cycle and the force criterion for structure relaxation were set at 10^{-6} eV and 10^{-2} eV/Å. The charge doping is simulated by varying the total number of electrons in the unit cell, with a compensating jellium background of opposite charge to maintain neutrality. Phonon dispersion curves were calculated by the supercell method (the $2 \times 2 \times 1$ supercell for NM, FM, and AFM states) using the PHONOPY package [45] with the energy convergence of 10^{-7} eV.

III. RESULTS AND DISCUSSION

To test the reliability and accuracy of this new method, we first investigated the 2D CrI_3 system. As shown in Fig. 1(a),

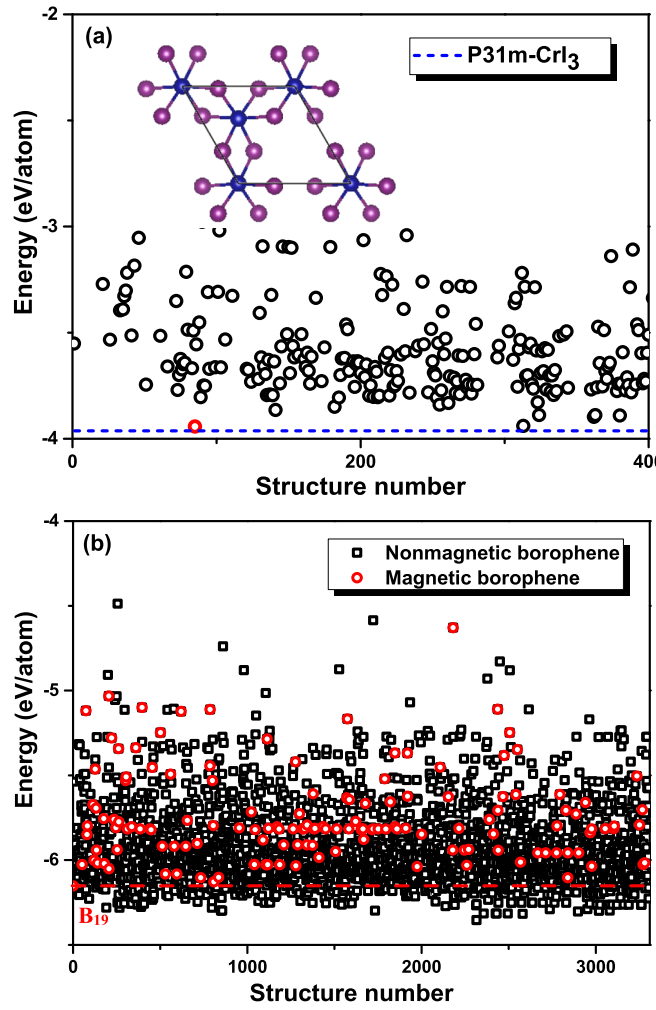

FIG. 1. (a) Energy evolution for 2D CrI_3 system during the magnetic evolutionary search. All of the structures are magnetic and the inset shows the most stable structure of $P3m1$–CrI_3. (b) Energy distribution of borophenes from the magnetic evolutionary search.

our calculations demonstrated that the most stable structure has ferromagnetic order and $P31m$ symmetry, and its lattice constants and magnetization (3 μ_B per Cr atom) are in good agreement with experimental results [2]. Compared with high-throughput computational screening [4,13,14], this search uncovered many new metastable magnetic structures which do not have analogous known parent bulk materials in the database, suggesting that our search is not biased by the database and thus offers a more complete sampling of the configurational space. We then applied this method to borophene. Both magnetic and nonmagnetic borophenes are unveiled in Fig. 1(b). Fewer than 300 magnetic borophenes were predicted among 3500 structures in total, after the removal of duplicate structures which were found more than once in the search. We also note that magnetic calculations may be numerically sensitive to the choice of computational parameters, and magnetism of some planar monolayers may disappear in more converged calculations because high density of states (DOS) at the Fermi level can be lowered by structural distortion. Since elemental boron prefers the NM state, all magnetic borophenes are metastable phases

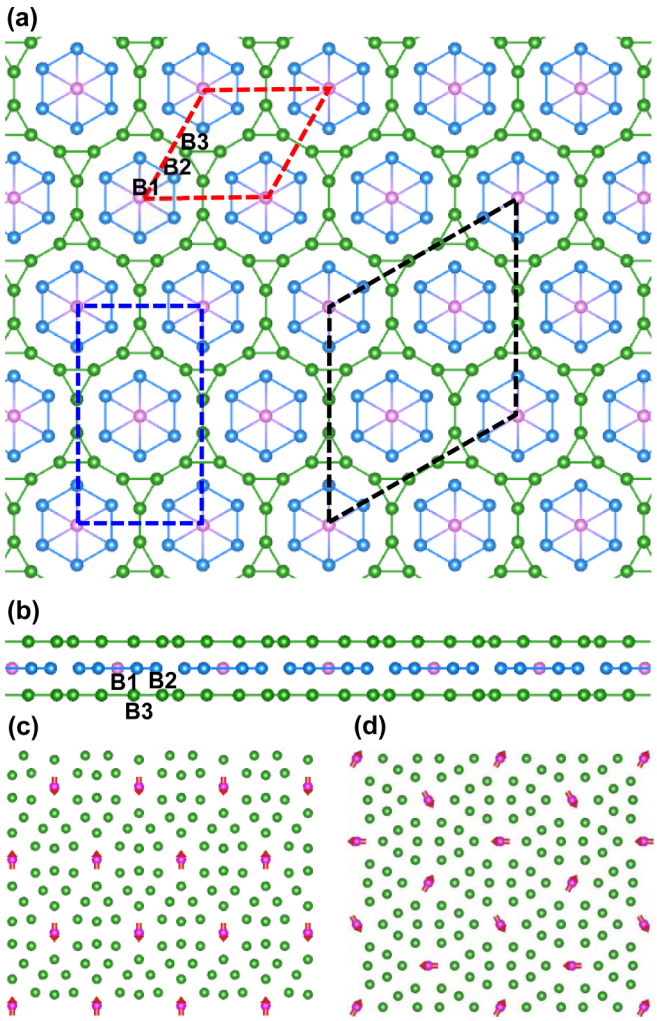

FIG. 2. (a) and (b) Top and side views of 19-$P6/mmm$ borophene. Some bonds among three layers are removed for clarity. Three inequivalent atomic positions (B1, B2, and B3) of NM structure are labeled. The dotted red, blue, and black lines indicate the lattices of NM, striped-AFM, and noncollinear 120° AFM (ncl-AFM) structures, respectively. (c) and (d) Striped-AFM and ncl-AFM; the pink arrows indicate the relative directions of their magnetic moments.

with respect to their ground-state structure. It is impractical to check the ground state (NM, FM, or AFM) for all magnetic structures because we only focus on several low-energy structures in which ferromagnetism persists, as they are more likely to be synthesized on a suitably chosen substrate. The most stable magnetic structure contains 19 atoms per unit cell (Fig. 2) and is designated as 19-$P6/mmm$ borophenes according to its symmetry. For 19-$P6/mmm$ borophene with NM order (NM 19-$P6/mmm$ borophene), the lattice parameters are $a = b = 6.033$ Å, and $c = 19.97$ Å. Three inequivalent atomic positions are B1 (0.0,0.0,0.5), B2 (0.362,0.181,0.5), and B3 (0.576,0.153,0.434), which form triatomic 2.64-Å-thick layers [see Figs. 2(a) and 2(b)]. The middle layer, through which a mirror plane passes, consists of isolated hexagonal B_7 clusters [meanwhile, leading to large empty spaces, see Fig. 2(a)], while the top and bottom layers, are composed of triangular units, and they connect together to form dodecagonal vacancies on top of the B_7 clusters, which forms a particular symmetric voided structure.

The calculated total energies for the 19-$P6/mmm$ borophene with striped-AFM [Fig. 2(c)], noncollinear 120° AFM order [ncl-AFM; see Figs. 2(a) and 2(d)], FM, and NM states are about −6.162, −6.162, −6.161, and −6.152 eV/atom, which are higher in energies than previously synthesized 2-$Pmmn$ (−6.19 eV/atom) [32], χ_3 (−6.24 eV/atom) [34], β_{12} (−6.23 eV/atom) [34], and α-sheet structures (−6.28 eV/atom) [20], but are lower in energy than graphenelike borophene (−5.42 eV/atom) [35], indicating that 19-$P6/mmm$ borophene is a metastable structure with the ground-state AFM order. There is only one magnetic atom per unit cell of FM 19-$P6/mmm$ borophene [Fig. 2(a)], which is located at the center of B_7 clusters (B1 atoms). The local magnetic moment of each B1 atom is about 1.0 μ_B. The geometry of B1 atoms forms a magnetic triangular lattice and thus many configurations including FM, striped-AFM, and ncl-AFM orders are considered (Fig. 2). The calculations show that the ncl-AFM phase, which is considerably (by 2.2 meV per 19 atoms, and 24.5 meV per 19 atoms) lower in energy than the striped-AFM and FM orders, respectively. Therefore, ncl-AFM borophene is the ground-state structure, which is an indirect-gap semiconductor with a bandgap of 0.54 eV [Fig. 3(a)]. Moreover, by mapping the DFT energy difference to the classical spin model, the nearest-neighbor exchange parameter J_1 is estimated to be −5.45 meV and the next nearest-neighbor exchange parameter J_2 is ∼−0.14 meV. J_1 is much bigger than J_2, indicating that 19-$P6/mmm$ borophene has a ground-state ncl-AFM structure, which is dominated by the AFM J_1 in the triangular lattice. However, under minor electron doping, the ncl-AFM phase is less stable than the striped-AFM and FM phases, and there is even an AFM-FM transition when doping concentration is higher than ∼0.006 electrons per atom (3.6×10^{13} cm^{-2}). Hence the ncl-AFM structure will not be discussed further in subsequent discussions for the doped cases.

Electronic band structure calculations show that NM 19-$P6/mmm$ borophene is metallic [Fig. 3(b)]. In contrast, striped-AFM and FM 19-$P6/mmm$ borophenes are semiconductors with an indirect bandgap of 0.41 eV and a direct bandgap of 0.18 eV, respectively [Figs. 3(c) and 3(d)]. The electronic stability, in terms of DOS at the Fermi level with the order of NM metal < FM or AFM semiconductor, is consistent with the energetic stability. To explore the physical origin of magnetism in striped-AFM borophene, we analyzed the orbital-resolved band structures as shown in Figs. 3(e) and 3(f). In Fig. 3(e), two flat bands around the Fermi level are primarily contributed by the p_z orbitals of magnetic B1 atoms. Between them, one flat band with majority spin is colored in pink, while the other with minority spin is colored in dark blue. Interestingly, there also exist two more flat bands in Fig. 3(f), which mainly originate from the other B1 atoms, but their spin characters are opposite. That is, two highest valence bands or two lowest conduction bands (flat bands) with opposite spin electrons offset each other [Figs. 3(e) and 3(f)] and thus, the whole structure exhibits AFM order. As mentioned above, these flat bands are dominated by the

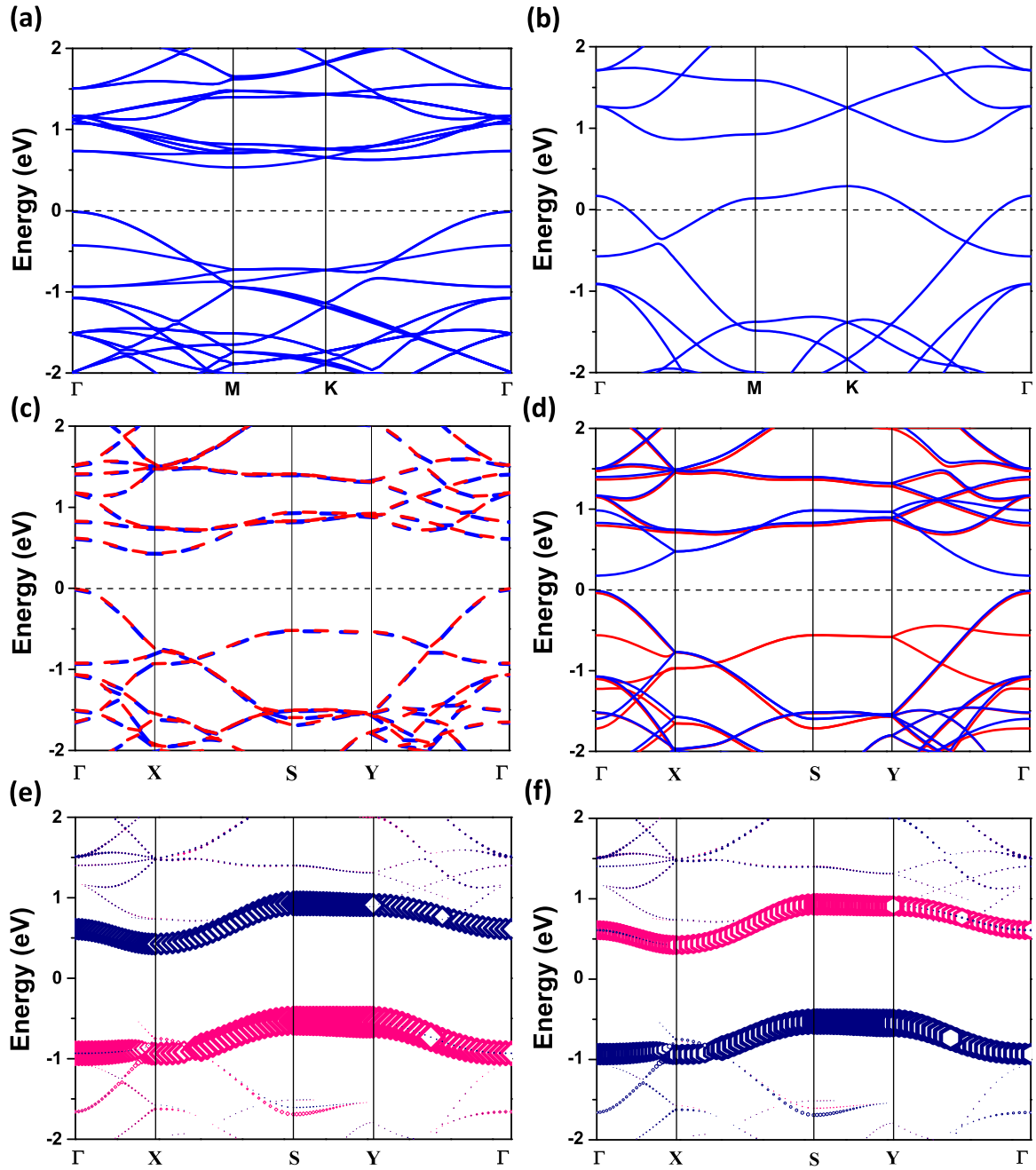

FIG. 3. Band structures of 19-$P6/mmm$ borophene with (a) ncl-AFM, (b) NM, (c) striped-AFM, and (d) FM structures. (e) The orbital-resolved band structures of striped-AFM 19-$P6/mmm$ borophene. Two flat bands dominated by the p_z orbitals primarily originate from one type of B1 atoms. The highest valence band with majority spin is colored in pink, and the lowest conduction band with minority spin is colored in dark blue. (f) These two flat bands mainly originate from the other magnetic B1 atoms of the striped-AFM state, but their spin electrons behave oppositely.

unpaired electrons (p_z orbitals), which can be confirmed by the spin charge density distribution [Figs. 4(a) and 4(b)]. Large bubblelike spin density maxima are localized on top of the B1 atoms (center of B_7 clusters). These bubbles represent the majority-spin (colored in red) and minority-spin electrons (colored in blue) and have the same size and shape due to mirror symmetry. The special arrangement of spin densities among B1 atoms in the plane are responsible for striped-AFM order. In addition, the electron localization function (ELF) of FM 19-$P6/mmm$ borophene in Figs. 4(c) and 4(d) shows that each B1 atom has an unpaired electron, and consequently has a local magnetic moment of 1 μ_B.

FM 19-$P6/mmm$ borophene is a direct narrow-gap semiconductor. As seen in Fig. 3(d), the lowest conduction band with minority spin is very close to the Fermi level along Γ-X and Γ-Y directions, while the conduction band with majority spin is relatively far from the Fermi level. Obviously, it may be tuned from the FM semiconductor to a FM half-metal

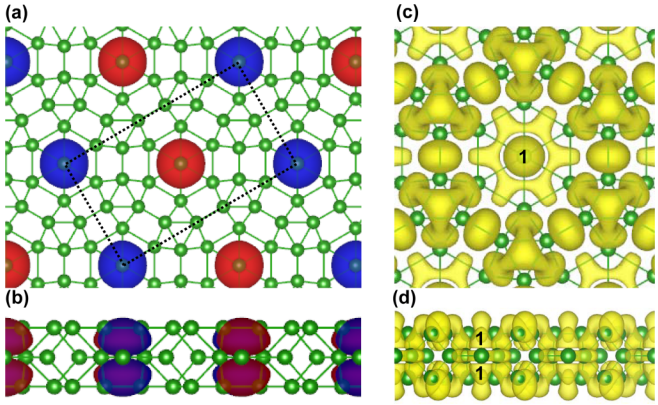

FIG. 4. (a) and (b) Top and side views of spin charge density of striped-AFM 19-*P*6/*mmm* borophene. The majority-spin charge density is colored in red, while the minority-spin charge density is colored in blue. The dotted lines indicate the rectangular lattice of the striped-AFM structure. (c) and (d) Top and side views of ELF of FM 19-*P*6/*mmm* borophene. The unpaired electrons are labeled as number 1 in (c) and (d).

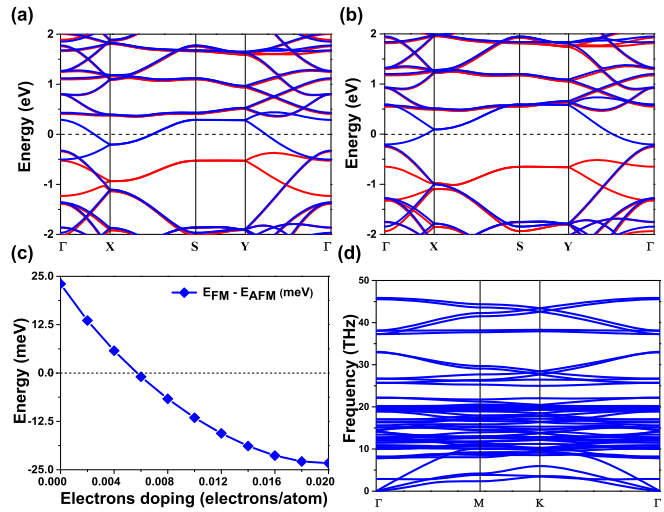

FIG. 5. (a) Band structure of FM 19-*P*6/*mmm* borophene with the electron doping concentration of 1.2×10^{14} cm^{-2}. (b) Band structure with the electron doping concentration of 4.8×10^{13} cm^{-2}. (c) Variation of the energy difference between FM and striped-AFM phases by finite electron doping. (d) Phonon dispersion curves of FM 19-*P*6/*mmm* borophene with doping of 0.02 electrons per atom.

by shifting the Fermi level upward a little, which can be realized by electron doping. Note that a charge doping of 10^{15} cm^{-2} had already been experimentally achieved in some 2D materials by a gate voltage [46]. For the electron doping of 0.02 (1.2×10^{14} cm^{-2}) and 0.008 (4.8×10^{13} cm^{-2}) electrons per atom [Figs. 5(a) and 5(b)], the bands in the majority and minority spin channels are separated, suggesting intrinsic ferromagnetism. Most importantly, minority spin channels are completely polarized, indicating that 19-*P*6/*mmm* borophene is a half-metal whose majority spin electrons behave like a semiconductor, while minority spin electrons display metallic conduction. All of these suggest that this structure may have significant potential applications in spintronics. Figure 5(c) shows the variation of the energy difference between FM and striped-AFM phases via electron doping from 0 to 1.2×10^{14} cm^{-2}. Actually, 19-*P*6/*mmm* borophene is a ground-state FM half-metal above the concentration of 0.006 electrons per atom. We also calculated the phonon dispersion curves with finite electron doping. The absence of imaginary frequencies in the phonon spectrum [Fig. 5(d)] suggests that the structure remains dynamically stable upon doping. Note that 19-*P*6/*mmm* borophene has a large unit cell and the excess electrons are dominantly distributed on the magnetic B1 atoms in both FM and striped-AFM states; the weak spurious electrostatic interaction can be canceled out, so the energy differences between the charged FM and striped-AFM states are correct [47].

Because of strong covalent B-B networks, borophenes are usually expected to be hard 2D materials, e.g., the in-plane Youngs modulus of 2-*Pmmn* borophene (398 GPa nm along the *a* axis), potentially rivals graphene (the strongest 2D material) at 340 GPa nm [32,48]. It is natural to study the mechanical properties of 19-*P*6/*mmm* borophene with different magnetic states. With its reconstructed rectangular lattice, using the standard Voigt notation, the elastic strain energy per unit area can be expressed as [49] $U_\epsilon = (1/2)C_{11}\epsilon_{xx}^2 + (1/2)C_{22}\epsilon_{yy}^2 + C_{12}\epsilon_{xx}\epsilon_{yy} + 2C_{66}\epsilon_{xy}^2$, where C_{11}, C_{22}, C_{12}, and C_{66} are the elastic constants, corresponding to second partial derivatives of the energy with respect to strain. The in-plane Young's modulus and Poisson's ratio can be derived from the elastic constants as $E_x = (C_{11}C_{22} - C_{12}C_{21})/C_{22}$, $E_y = (C_{11}C_{22} - C_{12}C_{21})/C_{11}$, $\nu_{xy} = C_{21}/C_{22}$, and $\nu_{yx} = C_{12}/C_{11}$. The calculated C_{11}, C_{22}, C_{12}, and C_{66} for striped-AFM 19-*P*6/*mmm* borophene are 227, 227, 143, and 42 GPa nm, so the Young's modulus is equal to $E_x = E_y = 137$ GPa nm, and the corresponding Poisson's ratio is equal to 0.63 [Fig. 6(a)], i.e., this borophene is much softer than previously reported structures [32,50]. In sharp contrast to the positive in-plane Poisson's ratio ($\nu_{xy} = \nu_{yx} = 0.63$), 19-*P*6/*mmm* borophene, regardless of its magnetic order, possesses an unexpected out-of-plane negative Poisson's ratio (NPR) when tensile strain was applied in the *x* (parallel to the *a* axis) and *y* (parallel to *b* axis) directions. As shown in Figs. 6(b) and 6(c), the out-of-plane strains ϵ_z of striped-AFM 19-*P*6/*mmm* borophene have a linear relationship with ϵ_x and ϵ_y, respectively. When it was compressed, the data were fitted to the function of $y = -0.119(-0.269)x$ in the $x(y)$ direction. Since the out-of-plane Poisson's ratio [51] is defined as $\nu_{zx} = -\partial\,\epsilon_z/\partial\,\epsilon_x$ or $\nu_{zy} = -\partial\,\epsilon_z/\partial\,\epsilon_y$, these results represent positive Poisson's ratios in both directions. Meanwhile for tension, the data were fitted to the function of $y = 0.381(0.162)x$, so they are $\nu_{zx} = -0.381$ and $\nu_{zy} = -0.162$, showing NPR effect, which is different from that of phosphorene or borophane (NPR for both tension and compression only either in the *y* or in the *x* direction) [52,53]. The length of specific B2-B3 bonds [named as *x* bonds, colored in red; see Fig. 6(d)] increases under tensile strain along the *x* direction, as do the other specific B2-B3 bonds [named as *y* bonds, colored in blue; see Fig. 6(d)] along the *y* direction. The slope of *x* bonds is more than that of *y* bonds, implying that *x* bonds elongate faster than *y* bonds upon stretching and resulting in $|\nu_{zx}| > |\nu_{zy}|$. Owing to very similar lattice constants among AFM, FM, and NM states, the ν_{zx} and ν_{zy} of NM (FM) 19-*P*6/*mmm* borophene are –0.416

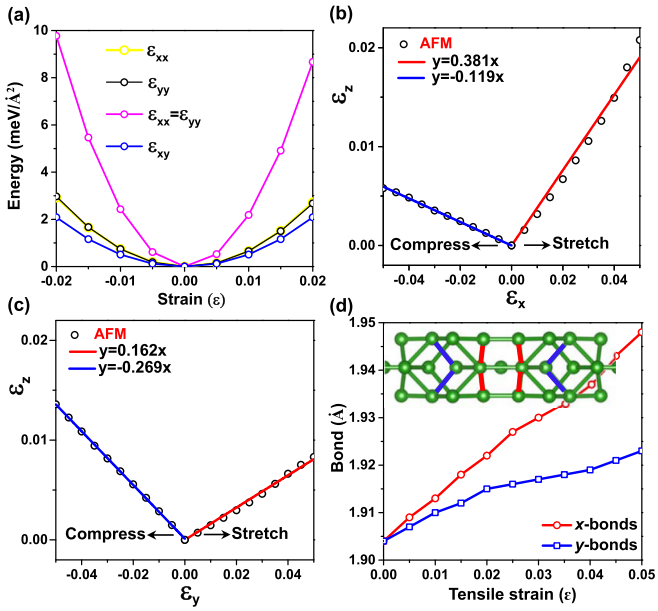

FIG. 6. Striped-AFM 19-*P*6/*mmm* borophene under strain. (a) Calculated total energy vs strain relation. (b) The Poisson's ratios as a function of uniaxial deformation of striped-AFM structure along the *x* direction. (c) Poisson's ratios as a function of uniaxial deformation of the AFM structure along the *y* direction. (d) The lengths of specific B2-B3 bonds as a function of uniaxial tensile strain. The inset shows the *x* bonds and *y* bonds, which are colored in red and blue, respectively.

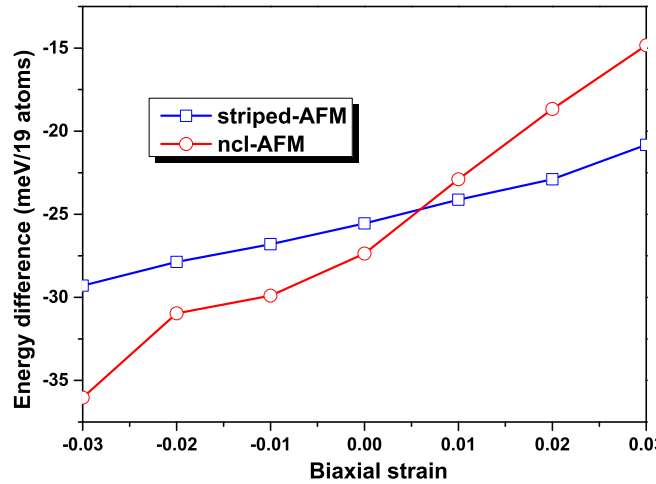

FIG. 7. The energy difference of striped-AFM, ncl-AFM refers to FM phases as a function of biaxial tensile (negative) or compressive strain (positive).

(–0.379) and –0.194 (–0.167) by using the same approach. Therefore, such exotic bonding configurations are responsible for the NPR effect [see the inset of Fig. 6(d)]. Finally, the energy difference of striped-AFM, ncl-AFM referring to the FM phases as a function of biaxial tensile (negative strain) or compressive strain (positive strain) was plotted in Fig. 7. It shows that the striped-AFM structure is the most stable phase among different states between the range of 1% and 3%, while the ncl-AFM structure is the most stable one under biaxial tensile strain.

IV. CONCLUSION

In conclusion, we have developed and applied a systematic evolutionary search for stable magnetic borophenes and identified that 19-*P*6/*mmm* borophene is a stable striped-AFM semiconductor, which not only can be further tuned into a half-metal, but also has intrinsic out-of-plane negative Poisson's ratios. The 19-*P*6/*mmm* borophene may be grown on suitable substrates of metals or transition-metal borides [54]. If magnetic borophenes can be realized in experiments, their outstanding properties make them promising candidates for application in spintronics and nanoelectromechanical devices simultaneously.

ACKNOWLEDGMENTS

This work was supported by the National Science Foundation of China (Grants No. 11674176, No. 11874224, No. 21803033, and No. 11604290), the National Key R&D Program of China (Grant No. YS2018YFA070119), and the Tianjin Science Foundation for Distinguished Young Scholars (Grant No. 17JCJQJC44400). A.R.O. thanks Russian Science Foundation (Grant No. 19-72-30043). Q.Z. is grateful for support from the National Nuclear Security Administration under the Stewardship Science Academic Alliances program through DOE Cooperative Agreement No. DE-NA0001982. G.G. thanks Ph.D. foundation by Yanshan University (Grant No. B970). X.D. and X.-F.Z thank the computing resources of Tianhe II and the support of Chinese National Supercomputer Center in Guangzhou.

[1] C. Gong, L. Li, Z. Li, H. Ji, A. Stern, Y. Xia, T. Cao, W. Bao, C. Wang, Y. Wang, Z. Q. Qiu, R. J. Cava, S. G. Louie, J. Xia, and X. Zhang, Nature (London) **546**, 265 (2017).

[2] B. Huang, G. Clark, E. Navarro-Moratalla, D. R. Klein, R. Cheng, K. L. Seyler, D. Zhong, E. Schmidgall, M. A. McGuire, D. H. Cobden, W. Yao, D. Xiao, P. Jarillo-Herrero, and X. Xu, Nature (London) **546**, 270 (2017).

[3] M. Bonilla, S. Kolekar, Y. Ma, H. C. Diaz, V. Kalappattil, R. Das, T. Eggers, H. R. Gutierrez, M.-H. Phan, and M. Batzill, Nat. Nanotechnol. **13**, 289 (2018).

[4] N. Mounet, M. Gibertini, P. Schwaller, D. Campi, A. Merkys, A. Marrazzo, T. Sohier, I. E. Castelli, A. Cepellotti, G. Pizzi, and N. Marzari, Nat. Nanotechnol. **13**, 246 (2018).

[5] S. Jiang, J. Shan, and K. F. Mak, Nat. Mater. **17**, 406 (2018).

[6] K. M. McCreary, A. G. Swartz, W. Han, J. Fabian, and R. K. Kawakami, Phys. Rev. Lett. **109**, 186604 (2012).

[7] A. Soumyanarayanan, N. Reyren, A. Fert, and C. Panagopoulos, Nature (London) **539**, 509 (2016).

[8] W.-Y. Tong, S.-J. Gong, X. Wan, and C.-G. Duan, Nat. Commun. **7**, 13612 (2016).

[9] M. A. McGuire, H. Dixit, V. R. Cooper, and B. C. Sales, Chem. Mater. **27**, 612 (2015).
[10] X. Li and J. Yang, J. Mater. Chem. C **2**, 7071 (2014).
[11] M.-W. Lin, H. L. Zhuang, J. Yan, T. Z. Ward, A. A. Puretzky, C. M. Rouleau, Z. Gai, L. Liang, V. Meunier, B. G. Sumpter, P. Ganesh, P. R. C. Kent, D. B. Geohegan, D. G. Mandrus, and K. Xiao, J. Mater. Chem. C **4**, 315 (2016).
[12] N. Sivadas, M. W. Daniels, R. H. Swendsen, S. Okamoto, and D. Xiao, Phys. Rev. B **91**, 235425 (2015).
[13] M. Ashton, J. Paul, S. B. Sinnott, and R. G. Hennig, Phys. Rev. Lett. **118**, 106101 (2017).
[14] G. Cheon, K.-A. N. Duerloo, A. D. Sendek, C. Porter, Y. Chen, and E. J. Reed, Nano Lett. **17**, 1915 (2017).
[15] K. S. Novoselov, A. K. Geim, S. V. Morozov, D. Jiang, Y. Zhang, S. V. Dubonos, I. V. Grigorieva, and A. A. Firsov, Science **306**, 666 (2004).
[16] O. V. Yazyev and L. Helm, Phys. Rev. B **75**, 125408 (2007).
[17] Y. Wang, Y. Huang, Y. Song, X. Zhang, Y. Ma, J. Liang, and Y. Chen, Nano Lett. **9**, 220 (2009).
[18] Z. Wang, C. Tang, R. Sachs, Y. Barlas, and J. Shi, Phys. Rev. Lett. **114**, 016603 (2015).
[19] H. González-Herrero, J. M. Gómez-Rodríguez, P. Mallet, M. Moaied, J. J. Palacios, C. Salgado, M. M. Ugeda, J.-Y. Veuillen, F. Yndurain, and I. Brihuega, Science **352**, 437 (2016).
[20] H. Tang and S. Ismail-Beigi, Phys. Rev. Lett. **99**, 115501 (2007).
[21] E. S. Penev, S. Bhowmick, A. Sadrzadeh, and B. I. Yakobson, Nano Lett. **12**, 2441 (2012).
[22] X. Wu, J. Dai, Y. Zhao, Z. Zhuo, J. Yang, and X. C. Zeng, ACS Nano **6**, 7443 (2012).
[23] X.-F. Zhou, X. Dong, A. R. Oganov, Q. Zhu, Y. Tian, and H.-T. Wang, Phys. Rev. Lett. **112**, 085502 (2014).
[24] Z. Zhang, Y. Yang, G. Gao, and B. I. Yakobson, Angew. Chem. Int. Ed. **54**, 13022 (2015).
[25] X.-F. Zhou, A. R. Oganov, Z. Wang, I. A. Popov, A. I. Boldyrev, and H.-T. Wang, Phys. Rev. B **93**, 085406 (2016).
[26] Y. Zhao, S. Zeng, and J. Ni, Phys. Rev. B **93**, 014502 (2016).
[27] W.-L. Li, T. Jian, X. Chen, T.-T. Chen, G. V. Lopez, J. Li, and L.-S. Wang, Angew. Chem. Int. Ed. **55**, 7358 (2016).
[28] T. Jian, W.-L. Li, X. Chen, T.-T. Chen, G. V. Lopez, J. Li, and L.-S. Wang, Chem. Sci. **7**, 7020 (2016).
[29] W.-L. Li, X. Chen, T. Jian, T.-T. Chen, J. Li, and L.-S. Wang, Nat. Rev. Chem. **1**, 0071 (2017).
[30] Z. A. Piazza, H.-S. Hu, W.-L. Li, Y.-F. Zhao, J. Li, and L.-S. Wang, Nat. Commun. **5**, 3113 (2014).
[31] W.-L. Li, Q. Chen, W.-J. Tian, H. Bai, Y.-F. Zhao, H.-S. Hu, J. Li, H.-J. Zhai, S.-D. Li, and L.-S. Wang, J. Am. Chem. Soc. **136**, 12257 (2014).
[32] A. J. Mannix, X.-F. Zhou, B. Kiraly, J. D. Wood, D. Alducin, B. D. Myers, X. Liu, B. L. Fisher, U. Santiago, J. R. Guest, M. J. Yacaman, A. Ponce, A. R. Oganov, M. C. Hersam, and N. P. Guisinger, Science **350**, 1513 (2015).
[33] G. Tai, T. Hu, Y. Zhou, X. Wang, J. Kong, T. Zeng, Y. You, and Q. Wang, Angew. Chem. Int. Ed. **127**, 15693 (2015).
[34] B. Feng, J. Zhang, Q. Zhong, W. Li, S. Li, H. Li, P. Cheng, S. Meng, L. Chen, and K. Wu, Nat. Chem. **8**, 563 (2016).
[35] W. Li, L. Kong, C. Chen, J. Gou, S. Sheng, W. Zhang, H. Li, L. Chen, P. Cheng, and K. Wu, Sci. Bull. **63**, 282 (2018).
[36] R. Wu, I. Drozdov, S. Eltinge, P. Zahl, S. Ismail-Beigi, I. Božović, and A. Gozar, Nat. Nanotechnol. **14**, 44 (2019).
[37] A. R. Oganov and C. W. Glass, J. Chem. Phys. **124**, 244704 (2006).
[38] W. Zhang, A. R. Oganov, A. F. Goncharov, Q. Zhu, S. E. Boulfelfel, A. O. Lyakhov, E. Stavrou, M. Somayazulu, V. B. Prakapenka, and Z. Konôpková, Science **342**, 1502 (2013).
[39] Q. Zhu, D. Y. Jung, A. R. Oganov, C. W. Glass, C. Gatti, and A. O. Lyakhov, Nat. Chem. **5**, 61 (2013).
[40] X. Dong, A. R. Oganov, A. F. Goncharov, E. Stavrou, S. Lobanov, G. Saleh, G.-R. Qian, Q. Zhu, C. Gatti, V. L. Deringer, R. Dronskowski, X.-F. Zhou, V. B. Prakapenka, Z. Konôpková, I. A. Popov, A. I. Boldyrev, and H. T. Wang, Nat. Chem. **9**, 440 (2017).
[41] https://uspex-team.org/en/uspex/documentation.
[42] P. E. Blöchl, Phys. Rev. B **50**, 17953 (1994).
[43] G. Kresse and J. Furthmüller, Phys. Rev. B **54**, 11169 (1996).
[44] J. P. Perdew, K. Burke, and M. Ernzerhof, Phys. Rev. Lett. **77**, 3865 (1996).
[45] A. Togo and I. Tanaka, Scr. Mater. **108**, 1 (2015).
[46] X. Li, X. Wu, and J. Yang, J. Am. Chem. Soc. **136**, 11065 (2014).
[47] J.-Y. Noh, H. Kim, and Y.-S. Kim, Phys. Rev. B **89**, 205417 (2014).
[48] C. Lee, X. Wei, J. W. Kysar, and J. Hone, Science **321**, 385 (2008).
[49] R. C. Andrew, R. E. Mapasha, A. M. Ukpong, and N. Chetty, Phys. Rev. B **85**, 125428 (2012).
[50] X.-L. He, X.-J. Weng, Y. Zhang, Z. Zhao, Z. Wang, B. Xu, A. R. Oganov, Y. Tian, X.-F. Zhou, and H.-T. Wang, FlatChem **7**, 34 (2018).
[51] Z. Gao, X. Dong, N. Li, and J. Ren, Nano Lett. **17**, 772 (2017).
[52] J.-W. Jiang and H. S. Park, Nat. Commun. **5**, 4727 (2014).
[53] L. Kou, Y. Ma, C. Tang, Z. Sun, A. Du, and C. Chen, Nano Lett. **16**, 7910 (2016).
[54] S. Suehara, T. Aizawa, and T. Sasaki, Phys. Rev. B **81**, 085423 (2010).